

# The role of E+A and post-starburst galaxies

## I. Models and model results

M. A. Falkenberg<sup>1\*</sup>, R. Kotulla<sup>2</sup> and U. Fritze<sup>2†</sup>

<sup>1</sup>*Institut für Astrophysik Göttingen, Georg-August Universität Göttingen, Friedrich-Hund-Platz 1, 37077, Göttingen*

<sup>2</sup>*Centre for Astrophysics Research, University of Hertfordshire, College Lane, Hatfield AL10 9AB, UK*

Accepted 2008 Month ??; Received 2008 Month ??; in original form 2008 Month ??

### ABSTRACT

Different compositions of galaxy types in the field in comparison to galaxy clusters as described by the morphology-density relation in the local universe is interpreted as a result of transformation processes from late- to early-type galaxies. This interpretation is supported by the Butcher-Oemler effect. We investigate E+A galaxies as an intermediate state between late-type galaxies in low density environments and early-type galaxies in high density environment to constrain the possible transformation processes.

For this purpose we model a grid of post-starburst galaxies by inducing a burst and/ or a halting of star formation on the normal evolution of spiral galaxies with our galaxy evolution code GALEV. From our models we find that the common E+A criteria exclude a significant number of post-starburst galaxies and propose that comparing their spectral energy distributions leads to a more sufficient method to investigate post-starburst galaxies. We predict that a higher number of E+A galaxies in the early universe can not be ascribed solely to a higher number of starburst, but is a result of a lower metallicity and a higher burst strength due to more gas content of the galaxies in the early universe. We find that even galaxies with a normal evolution without a starburst have a  $H\delta$ -strong phase at early galaxy ages.

**Key words:** Galaxies: evolution – Galaxies: formation – Galaxies: interactions – Galaxies: starburst – Galaxies: clusters: general

## 1 INTRODUCTION

The composition of galaxy types is different in the field (=low galaxy density environments) as compared to galaxy clusters (=high galaxy density environment). In the local universe this e.g. is described by the morphology-density (MD) relation (Dressler 1980; Oemler 1974). The higher the projected surface density of galaxies within an area, the higher is the fraction of early-type galaxies and the lower is the fraction of late-type galaxies (Dressler et al. 1997). The field is rich in spirals and irregular galaxies, while in clusters mainly S0s, dSphs and dEs are found. Butcher and Oemler were the first to report a high fraction of blue galaxies in distant clusters as compared to local ones (BO effect, see Butcher & Oemler (1984, 1978); Ellingson et al. (2001); Kodama & Bower (2001). Since galaxy clusters grow by continuous accretion of the field galaxies, this difference is not caused by different formation histories but is due to a transformation that takes place during the lifetime of a galaxy (Couch et al. 1994; Dressler et al. 1994). This interpretation is supported by findings that the fraction of ellipticals remains constant in clusters of different redshift, while the fraction of spirals increases and the fraction

of S0 galaxies correspondingly decreases with increasing redshift (see Fasano et al. 2000). When galaxies encounter a high density environment like a galaxy cluster the star formation (SF) is suppressed causing an evolution from late to early spectral types for these galaxies. This shows that environment plays a crucial role in the evolution of galaxies. While in earlier times it was believed that galaxy transformation takes only place in clusters and is related to the Intra Cluster Medium (ICM), today we know that galaxy properties like the SF activity, the H I content and morphological type depend on the local galaxy density in general and the ICM cannot be the only explanation to it. When spectra of the blue population of galaxies in clusters were investigated, most BO galaxy spectra showed strong emission lines typical of blue star forming galaxies. However some of the blue galaxies were discovered to show spectra with strong Balmer absorption lines, but no emission lines (Couch & Sharples 1987). These spectra are different from the spectra of any normal Hubble type galaxy and were named E+A galaxies. In many clusters, these E+A galaxies constitute a large fraction of the blue galaxy population (Barger et al. 1996; Poggianti & Barbaro 1996). Some red galaxies in clusters were also discovered to show strong Balmer absorption lines. This effect is called the "spectroscopic BO-effect". X-ray observations have shown that E+A galaxies can be found near the edges of infalling structures in clusters located in an area between early-type

\* E-mail: atyra@astro.physik.uni-goettingen.de

† E-mail: r.kotulla@herts.ac.uk, u.fritze@herts.ac.uk

galaxies in the central cluster regions and late-type galaxies in the field and cluster outskirts (Poggianti et al. 2004). Investigations of Helmboldt (2007) show that the gas content of E+A galaxies on average lies between gas-rich disk galaxies and typical gas poor E/S0 galaxies.

Several processes have been proposed as mechanisms for the transformation of galaxies in cluster environments. The most common ones are mergers, harassment, gas stripping and strangulation. *Harassment* is an effect of tidal forces caused by a series of many weak galaxy-galaxy encounters with high relative velocities. The encountering galaxies are influenced by each other's gravitational field. They strip off stars and gas from each other's outer regions and weaken or even destroy their internal stabilities and disks. This can result in a star burst and/or the termination of SF on a long timescale of 1-5 Gyr. Harassment is a theoretically motivated mechanism, which has been observed in numerical simulations (see Moore et al. 1998; Richstone 1976). It is believed to play an important role in rich galaxy clusters. *Gas stripping* describes interactions between the gas in the disk of a galaxy and the hot and dense Intra Cluster Medium (ICM) detected in X-ray observations (Gunn & Gott 1972; Quilis et al. 2000). Some examples are viscous stripping, thermal evaporation, and ram pressure stripping. The effect is strongest when the relative velocities are high and the ICM is very dense, i.e. it is expected to take place in the central cluster regions. Ram pressure stripping has been observed (see Cayatte et al. 1990; Bravo-Alfaro et al. 2000; Gavazzi et al. 2003) and has an indirect effect on the morphology of a galaxy as it leads to a truncation of SF on a timescale of  $\geq 0.1$  Gyr with possibly a small burst prior to the truncation. When SF stops in a spiral galaxy, its disk starts fading considerably, and the galaxy evolves towards higher bulge to disk luminosity fractions, hence towards an earlier morphological type. If instead of disk gas the low density halo gas gets stripped from a galaxy falling into a cluster gravitational potential, *strangulation* has been proposed to occur. The halo is a gas reservoir and feeds the SF. Its removal results in a termination of SF on a timescale of  $\geq 1.0$  Gyr. The morphology is again influenced indirectly through the halting of SF. *Galaxy mergers* are galaxy-galaxy interactions which are most efficient at low relative velocities (Toomre & Toomre 1972; Mihos 2004). Mergers are therefore more frequent in galaxy groups than in clusters. The relative velocities of galaxies in groups are comparable to the velocities of the stars within the galaxy, a condition very favorable for merging, while in clusters the galaxy velocity dispersion is higher by factors  $\geq 10$ . If the interacting galaxies are gas-rich, a major starburst can be triggered, followed by a truncation of the star formation on a timescale of  $\sim 0.1 - 0.4$  Gyr. Observations about HI gas in E+A galaxies indicate galaxy-galaxy interactions or mergers as possible transformation mechanisms (Chang et al. 2001; Buyle et al. 2008). Enhanced merging within groups falling into clusters has been evolved as possible explanation of the observation that the galaxy population changes already at relatively large distances from the cluster center around  $3 R_{vir}$  (see Verdugo et al. 2008), where the ICM is not yet expected to have a strong effect. While starbursts in the course of tidal stripping of galaxies are at most expected to be weak, starbursts accompanying gas-rich mergers have been found to be very strong in some cases. All of these transformation scenarios result in both a morphological and a spectral transformation of the infalling spiral-rich field galaxy population. The E+A galaxies seem to be a missing link in the process of spiral galaxies evolving into early-type galaxies and the investigation of this galaxy type will lead to a better understanding of galaxy evolution. With surveys like SDSS, CNOC and LCRS, E+A galaxies were also found

in the field, which indicates that transformation of galaxies does not only take place in clusters, but also in enhanced density environments outside clusters (Zabludoff et al. 1996; Balogh et al. 1999). The respective timescales for the transformation scenarios need not to be the same and are still largely unexplored. The Hubble Space Telescope (HST) makes it possible to also study the morphological evolution of galaxies and compare the timescales of spectroscopic and morphological transformation.

## 1.1 E+A Galaxies

The spectra of E+A galaxies look like a superposition of a passive continuum spectrum of an elliptical galaxy (or an ensemble of K-type stars) without emission lines but with deep Balmer absorption lines typical for A stars. Therefore this class of galaxies was named E+A or k+a, which is only a spectral but not a morphological classification. A lack of emission lines like in the E+A galaxies indicates a lack of actively star-forming regions (Gómez et al. 2003). Usually the equivalent width of the emission line [O II] at 3727 Å is measured as an indicator of current star formation. On the other hand, Balmer absorption lines are an indicator for recent SF. They are produced by a dominance of intermediate age stars in the galaxy and are strongest for A0 stars. A-type stars begin to dominate the light of a galaxy about 0.5 Gyr after SF stops and have a lifetime of about 3 Gyr. Their signature in the spectrum can best be seen 1-1.5 Gyr after active SF (Leonardi & Rose 1996; Poggianti 2004). This knowledge about the origin of the Balmer absorption lines has led to the conclusion that E+A galaxies are post-starforming, passive galaxies which had their last star formation about 1-1.5 Gyr ago (Couch & Sharples 1987; Poggianti 2004). A starburst, i.e. a short-term increase in the SF activity, preceding the halting of SF is required in galaxies with strong Balmer lines. The strength of the Balmer lines is a measure of the strength of the recent SF.

The exact definitions of E+A galaxies varies among different authors. Yang et al. (2004) set the threshold for E+A galaxies at an  $EW[(H\beta, H\gamma, H\delta)] > 5.5 \text{ \AA}$ , while Poggianti et al. (2004) classify galaxies with  $EW(H\delta) > 3 \text{ \AA}$  as E+A galaxies and propose an additional threshold of  $EW(H\delta) > 5 \text{ \AA}$  for *strong* E+A galaxies. For the  $EW([O II])$ , a threshold around 2-5 Å is usually adopted, depending on the detection limit. In this work, we chose the H $\delta$ -line at 4100 Å as an indicator for recent SF, because this line is less affected by emission filling than lower order lines. The threshold for E+A galaxies is set to  $EW(H\delta) \geq 5 \text{ \AA}$ .

## 1.2 Goal of this Work

In this work we will investigate different scenarios which are thought to be responsible for the transformation from one galaxy type to another. Our focus is on E+A galaxies, which are believed to be a transition stage in galaxy transformation from low density environment spirals to high density environment S0 galaxies. For this purpose a grid of galaxy models is calculated with our galaxy evolution code GALEV, which models the photometric, spectral and chemical evolution of a galaxy. With starbursts and/or the halting of the star formation we can simulate the effect of the different processes of galaxy transformation on the SFR. The GALEV code does not take into account the dynamical evolution or spatial resolution. We only consider here the effect of the various transformation scenarios on the SFR and on the evolution of the integral spectrum and colors of a galaxy that it induces.

Our goal is to identify possible progenitors and successors of

E+A galaxies and investigate their spectra, luminosities and colors, in order to understand the role of the different transformation processes. The paper is organized as follows. In Sect. 2 we will describe our galaxy evolution code GALEV. Sect. 3 gives the results that can be drawn from our calculated grid of undisturbed and post-starburst galaxies. In Sect. 4 a conclusion is given. In a companion paper (Falkenberg et al. 2009, hereafter Paper II) we will investigate the Spectral Energy Distributions (SEDs) of our post-starburst galaxy models and make a comparison with observations.

## 2 MODEL DESCRIPTION

### 2.1 Undisturbed Galaxies

The GALEV code starts from a gas cloud of primordial abundance and a given initial mass. A given star formation rate (SFR)  $\psi(t)$  determines the total amount of stars formed in each time step. The mass distribution of the new stars is determined by an initial mass function (IMF)  $\phi$ . The evolution of each star in the Hertzsprung-Russell diagram (HRD) is traced with a set of stellar isochrones for 5 different metallicities. We have used the latest isochrones from the Padova group (Bertelli et al. 1994; Girardi et al. 2003) that contain 26 stellar masses with 1067 evolutionary stages including the thermal-pulsing AGB phase. Each stage is determined by effective temperature  $T_{\text{eff}}$ , luminosity  $\frac{L_{\text{bol}}}{L_{\text{bol},\odot}}$  and life time. At any timestep the galaxy is described by a set of weighted isochrones. With a library of stellar model atmosphere spectra, it is possible to calculate a spectrum for each isochrone. The adopted stellar library contains spectra from the UV to the NIR for all spectral types and luminosity classes for 5 metallicities (Lejeune et al. 1998). Summing the isochrone spectra for each metallicity, weighted by the SFR at the birth of the stars, and adding the spectra of the various metallicity subpopulations, we synthesize an integrated galaxy spectrum. For details about the GALEV code see Anders & Fritze-v. Alvensleben (2003).

For undisturbed spiral galaxy models we tie the SFR  $\psi(t)$  to the evolving gas content  $G(t)$  with  $G(t) \propto \psi(t)$  and determine efficiency parameters for spectral galaxy types Sa, Sb, Sc, Sd as to obtain, for a Salpeter IMF, at an age of 12 Gyr agreement with observations in the UV, optical and NIR. The initial gas masses, and hence the initial value of the SFR are chosen as to obtain, after 12 Gyr of evolution, the average observed B-band luminosities of the respective galaxy types Sa, Sb, Sc, Sd as determined for Virgo by Sandage et al. (1985). Fig. 1 shows the evolution of the SFR  $\psi(t)$  over time for the undisturbed Sa, Sb, Sc and Sd galaxy models.

We stress that our Sa, Sb, Sc, Sd galaxy models are meant to describe *spectral galaxy types*. The observed one-to-one correspondence between spectral and morphological galaxy types in the local universe might, of course, not hold back until arbitrary high redshifts.

The UV, optical and NIR colors, the spectra, the gas content and the chemical abundances are in agreement with observations as shown in Bicker et al. (2004). However in contrast to Bicker et al. (2004), in this work the metallicity of the stellar population is held constant at  $Z = 0.008$ , i.e. at about half-solar metallicity. Half-solar metallicity is a typical value for spiral galaxies in the local and moderately distant universe (Tremonti et al. 2004; Zaritsky et al. 1994). There are several reasons why closed-box models used in the chemically consistent description do not appear appropriate for investigating E+A galaxies: 1.) E+A are likely to be caused by major mergers of two gas-rich, i.e. late-type spirals (Kaviraj et al. 2007) in

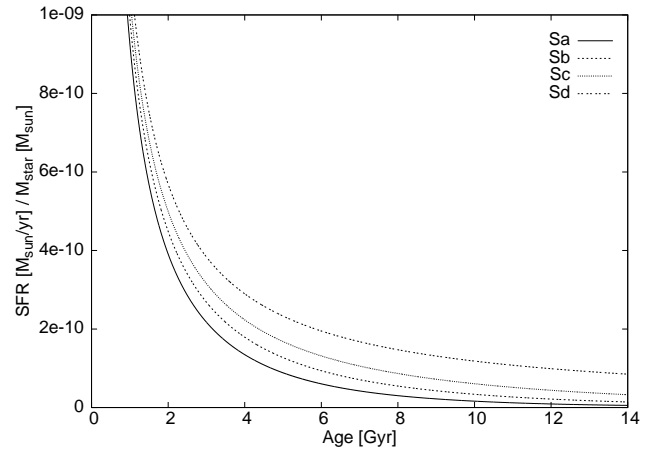


**Figure 1.** Time evolution of the SFR of the undisturbed Sa, Sb, Sc and Sd galaxy models.

order to reproduce the large fraction of newly formed stars. Those mergers are by definition no closed-boxes, so that assuming closed box models are not justified. 2.) Other galaxy transformation processes in clusters are as well expected to be accompanied by mass loss. 3.) Bursts are likely to be associated with galactic outflows, also making the assumptions of closed-boxes invalid. Further support comes from the non-detections of many E+As in HI, implying low remaining gas-masses (Goto 2004; Liu et al. 2007).

The GALEV code does not take into account that galaxies might contain a high amount of dust, which has a reddening effect on the integral colors. However, the majority of post-starburst galaxies are believed to contain no or only little amount of dust (Balogh et al. 2005; Goto 2004) and therefore can be modelled accurately with GALEV. Some post-starburst galaxies, on the other hand seem to still contain some dust. Those galaxies, of course, cannot appropriately be described by our dust-free models

Our spectra do not have enough resolution to quantitatively analyze any lines. While we implemented a calculation for the [O III] emission lines into the GALEV code, for the analysis of the Balmer lines we used the Lick calibration to calculate the line strength separately (see Sect. 2.3 and 2.2).

### 2.2 Lick Indices

GALEV models include Lick indices, which are spectral absorption features in well-defined wavelength ranges. The names of the 25 Lick indices refer to the most prominent line in the wavelength range of each individual index. Most indices are measured in terms of equivalent widths with the following definition:

$$\text{EW}[\text{\AA}] = \int_{\lambda_1}^{\lambda_2} \frac{F_C(\lambda) - F_I(\lambda)}{F_C(\lambda)} d\lambda \quad (1)$$

Here  $F_I$  is the flux for the index between two wavelengths  $\lambda_1$  and  $\lambda_2$ .  $F_C$  is the continuum flux, calculated from two "pseudo-continua" with wavelength ranges defined to the left and right of the central index bandpass.

We model the Lick indices for individual stars on the basis of polynomial fitting functions of Worthey et al. (1994) and Worthey & Ottaviani (1997). The index strength for the isochrones are derived by integrating and weighting with the IMF. With the isochrones from all contributions at each timestep, we get weighted Lick indices for the galaxy (for detail see Lilly & Fritze 2006).

**Table 1.** Wavelength ranges for the Lick indices of the Balmer lines.

Index	Blue continuum	Index bandpass	Red continuum
H $\beta$	4827.875–4847.875	4847.875–4876.625	4876.625–4891.625
H $\gamma$	4283.500–4319.750	4319.750–4363.500	4367.250–4419.750
H $\delta_A$	4041.600–4079.750	4083.500–4122.250	4128.500–4161.000
H $\delta_F$	4057.250–4088.500	4091.000–4112.250	4114.750–4137.250

In this work, we only investigate the Balmer line indices H $\beta$ , H $\gamma$ , H $\delta_F$  and in particular H $\delta_A$ . In Tab. 1 the bandpass definitions of the index bandpasses and the pseudo-continua are listed (see Trager et al. 1998).

### 2.3 [O II]-Emission Lines at 3727Å

We implemented into the code a calculation of the EW([O II]) for the [O II]-line at 3727 Å, which is an indicator of current SFR and is used for the definition of E+A galaxies. The EW([O II]) can be modelled from the SFR and B-band luminosity with the following relations given by Kennicutt (1992b):

$$\text{SFR} (M_{\odot} \text{ yr}^{-1}) \simeq 5 \cdot 10^{-41} L([\text{O II}]) \quad (2)$$

and

$$L([\text{O II}]) \sim 1.4 \pm 0.3 \cdot 10^{29} \frac{L_B}{L_B(\odot)} \text{EW}([\text{O II}]) \text{ ergs}^{-1} \quad (3)$$

### 2.4 Galaxy Transformation Scenarios

The interactions of galaxies, as described in Sect. 1 have different characteristic influences on the SFR of a galaxy. Only the effects on the SFR will be the subject of this investigation. The dynamical and morphological transformation, which accompany galaxy transformation processes are beyond the scope of this work.

The various mechanisms are realized with GALEV by inducing a sudden change in the SFR of a normal undisturbed galaxy. Three different ways of changing the SFR can describe the four important mechanisms of galaxy interaction. 1.) A truncation of the SFR on a short timescale, 2.) a termination of SF on a long timescale, and 3.) a burst, which is a rapid short-term increase in SFR before a truncation or termination of the SFR. Our assumption of a sudden increase is compatible with the findings from Bekki et al. (2005), who used a 2-D dynamical simulation of spiral mergers and also found a very sharp rise in SFR at the onset of the burst followed by an exponentially declining SFR. Possible scenarios for the decline in SFR after a burst are exhaustion of the fuel for SF, the heating and stirring of the ISM during the burst or the expansion of the remaining gas by a large scale galactic wind. We chose spiral type galaxies as most likely progenitors for E+A galaxies. Bursts of SF at various times  $t_{\text{burst}}$ , with various burst strengths  $b$  and decline timescales  $\tau$  are induced in the different spiral type models to simulate the different burst and truncation scenarios. Tab. 2 shows how the effects of the different transformation processes are described by our models in their impact on the SFR.

To model a burst, the SFR of an undisturbed spiral is set to a value  $\psi_{\text{burst}}$  at time  $t_{\text{burst}}$ . The decline after the burst is described by an exponential law with a decline timescale  $\tau$ .

$$\psi(t \geq t_{\text{burst}}) = \frac{\psi_{\text{burst}}}{e^{t-t_{\text{burst}}/\tau}} \quad (4)$$

The maximum burst SFR  $\psi_{\text{burst}}$  together with  $\tau$  determines the

**Table 2.** Effects on the SFR and timescales for the halting of SF for galaxy interactions.

Interaction	Effect on SFR	$\tau$ [Gyr]
merger	burst with truncation	0.1, 0.3
harassment	(burst and) termination	1.0
gas stripping	(burst and) truncation	0.1, 0.3
strangulation	termination	1.0

**Table 3.** Comparison of the burst strengths obtained for three different definitions in the literature.

Type	$t_{\text{burst}}$ [Gyr]	$\tau$ [Gyr]	$b$ [%]	$b_s$	$b_{\psi}$
Sa	11	0.1	30	0.01	7.13
		1.0	30	0.01	0.71
	9	1.0	70	0.02	1.66
		1.0	30	0.01	0.60
	6	1.0	70	0.03	1.40
		1.0	30	0.04	0.71
Sd	11	1.0	30	0.24	2.22
		1.0	70	0.56	5.17
	9	1.0	30	0.36	2.71
		1.0	70	0.83	6.33
	6	1.0	30	0.68	3.46
		1.0	70	1.58	8.08

burst strength  $b$ . In our models  $b$  is primarily defined as the fraction of the remaining gas at  $t_{\text{burst}}$  that is consumed in the burst

$$b := \frac{\Delta G}{G(t_{\text{burst}})} \quad (5)$$

$G(t_{\text{burst}})$  is the gas mass at the beginning of the burst,  $\Delta G$  the fraction of  $G(t_{\text{burst}})$  that is consumed for SF during the burst. Other definitions of burst strength also found in the literature are based on the increase of stellar mass  $S$  (6) or the SFR enhancement (7).

$$b_s = \frac{\Delta S}{S} \quad (6)$$

or

$$b_{\psi} = \frac{\psi_{\text{burst}}}{\psi_i} \quad (7)$$

with  $\psi_i$  as the SFR just before the burst. In Tab. 3, the burst strength values from these three definitions are compared for a few examples.

A truncation or a termination of SFR without a preceding starburst is implemented with a similar exponential law starting from the SF at the beginning of the truncation/termination  $t_{\text{trunc}}$ .

We have calculated a grid for the spiral galaxy types Sa, Sb, Sc and Sd each with burst strengths of  $b=0\%$ , 30%, 50% and 70%, onsets of the bursts at galaxy ages of 3 Gyr, 6 Gyr, 9 Gyr and 11 Gyr and decline times of 0.1 Gyr, 0.3 Gyr and 1.0 Gyr. A burst strength  $b=0\%$  stands for pure truncation or termination of SF depending on the decline time. In the following we will refer to galaxies with starbursts, SF truncation and SF termination *together* as (post-)starburst galaxies, since one can describe a truncation or termination as starburst with a burst strength of 0%.



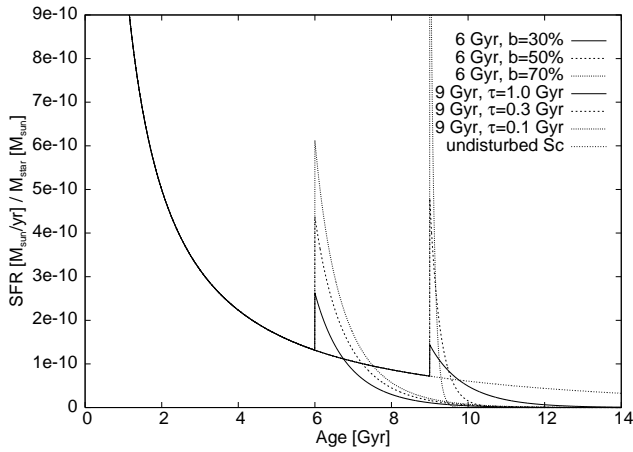


**Figure 2.** Time evolution of the SFR of Sc galaxy models with bursts. The bursts beginning at 6 Gyr have different burst strengths of 30%, 50% and 70%, but the same decline times of 1.0 Gyr. The bursts beginning at 9 Gyr have different decline times of 0.1, 0.3 and 1.0 Gyr, but the same burst strength of 30%.

## 2.5 The SFRs of Starburst Galaxy Models

In Fig. 2 the evolution of the SFR  $\psi(t)$  for an Sc galaxy model with various burst scenarios is shown in contrast to an undisturbed Sc galaxy.

Three bursts beginning at 6 Gyr with the same decline times of  $\tau=1.0$  Gyr but different burst strengths of  $b=30\%$ , 50% and 70% are compared. From the three burst scenarios beginning at 9 Gyr on the right, it can be seen that at a given gas consumption rate the decline time, i.e. the transformation scenario, influences the maximum of the SFR in the burst significantly. At fixed  $\tau$  a burst with higher gas consumption has a larger  $\psi_{\text{burst}}$ . While a long decline time typical for mild harassment or strangulation results only in a small maximum burst SFR  $\psi_{\text{burst}}$ , a medium or short decline time caused by gas stripping or by a merger produces much higher burst SFRs when consuming the same amount of gas. It can also be seen that the burst SFR significantly depends on the onset time of the burst. A later beginning implies that the galaxy has already consumed more of its gas content. Therefore a burst at a galaxy age of 9 or 11 Gyr will not have as high a SFR as a burst at 6 Gyr.

The scenarios in Fig. 3, again compared to an undisturbed Sc model, show the truncation/termination of the SF of an Sc model at an age of 6 Gyr on different timescales  $\tau$ . The models with  $\tau=0.1$  Gyr and  $\tau=0.3$  Gyr simulate a truncation after a merger or the stripping of gas from the disk. The model with  $\tau=1.0$  Gyr is a termination of SF as caused by galaxy harassment or strangulation.

## 3 RESULTS

### 3.1 Lick Index $H\delta$ of Undisturbed Galaxies

In this Sect. we investigate the evolution of the  $EW(H\delta)$  for our undisturbed galaxy models for spectral types Sa, Sb, Sc to later compare them with the transformation models. In Fig. 4 we plot the  $EW(H\delta)$  as a function of galaxy age. The horizontal line in Fig. 4 indicates the  $5 \text{ \AA}$  threshold, separating  $H\delta$ -strong from non- $H\delta$ -strong galaxy models. Galaxies lying above this line during any time of their evolution would be observationally classified as  $H\delta$ -strong galaxies and therefore fulfill one of the two criteria for the definition of E+A galaxies.

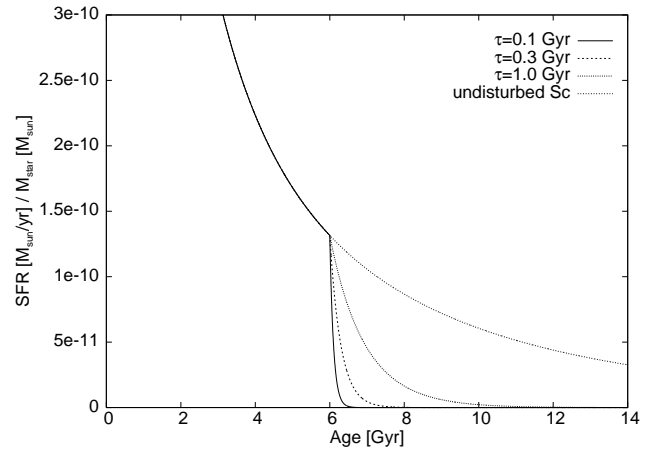


**Figure 3.** Time evolution of the SFR of Sc type spiral galaxies with a halting of SFR on different timescales of 0.1, 0.3 and 1.0 Gyr, but with the same onset at 6 Gyr.

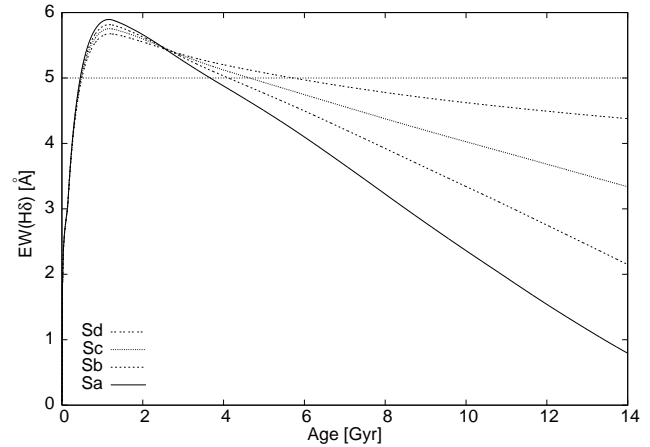


**Figure 4.** Time evolution of the  $EW(H\delta)$  of undisturbed spiral galaxies. The horizontal line marks the  $5 \text{ \AA}$  threshold.

Fig. 4 shows that the  $EW(H\delta)$  grows fast after the onset of SF and reaches a maximum value around 1 Gyr. The  $EW(H\delta)$  of  $5.5\text{--}6 \text{ \AA}$  of the different galaxy types declines on different timescales.

It is to note that all undisturbed normal spiral galaxy models lie above the threshold and therefore have an  $H\delta$ -strong phase early in their evolution lasting until ages of 3 to almost 6 Gyr, i.e. to redshifts  $z \sim 2\text{--}1$  for Sa and Sd types, respectively. The values for  $EW([O\text{II}])$  and for  $EW(H\delta)$  for an Sa and an Sd model at 1.5 Gyr are listed in Tab. 4. The values for the  $EW([O\text{II}])$  are too high for the undisturbed galaxies in the  $H\delta$ -strong phase to classify them as E+A galaxies.

The values for  $EW(H\delta)$  and  $EW([O\text{II}])$  between ages of 1.5

**Table 4.**  $EW([O\text{II}])$  and  $EW(H\delta)$  of Sa and Sd model at ages of 1.5 Gyr, 4 Gyr (Sa) and 6 Gyr (Sd), respectively.

Type	Age [Gyr]	$EW([O\text{II}])[\text{\AA}]$	$EW(H\delta)[\text{\AA}]$
Sa	1.5	37.25	5.83
	4	26.98	4.88
Sd	1.5	42.06	5.64
	6	33.63	4.97

and 6 Gyr are a striking result, because it indicates that galaxies which only follow the normal evolution, all go through a phase in which they have strong H $\delta$ -lines without having a starburst. Not taking this result into account in analyses of high redshift galaxies leads to an underestimate of their emission lines, which are influenced by the Balmer absorption lines, for example the  $H\alpha$  and  $H\beta$ , and of the SFR derived from those.

From Fig. 4 it is also obvious that a lower threshold of 3 Å for EW(H $\delta$ ) as sometimes used in literature is not appropriate because the undisturbed galaxy models have values of EW(H $\delta$ )  $\geq$  3 Å for at least 9 Gyr, i.e. until  $z \sim 0.4$ .

### 3.2 Lick Index H $\delta$ for Post-Starburst Galaxies

For the discussion of the E+A galaxies, we start with the investigation of EW(H $\delta$ ) and EW([O II]) of our starburst models, because the presence of strong Balmer absorption lines and the absence of emission lines are the two criteria to distinguish between E+A and non-E+A galaxy models. In Sect. 3.2 we investigate which of our models are H $\delta$ -strong by looking at the EW(H $\delta$ ) as a function of time and in Sect. 3.4 we investigate the time evolution of EW([O II]).

In Figs. 5 and 6 the evolution of the EW(H $\delta$ ) of different burst and truncation models are represented. Fig. 5 shows an Sd and an Sa model with a burst at a galaxy age of 6 Gyr as well as an Sa model with a burst at a galaxy age of 9 Gyr and 11 Gyr. For all four models the burst strength  $b$  amounts to 70% and the decline time is  $\tau=0.1$  Gyr. For the two models with a burst at 6 Gyr, the EW(H $\delta$ ) drops strongly at the onset of the burst before it grows and crosses the threshold of 5 Å. This drop is caused by the dominance of young burst stars, which do not show strong Balmer lines. The H $\delta$ -strong phase starts 0.2 Gyr after the onset of the burst and lasts for 0.5 Gyr (Sa) to 1.1 Gyr (Sd). After the H $\delta$ -strong phase the EW(H $\delta$ ) declines very fast and becomes smaller than in the undisturbed galaxies. In contrast to the undisturbed galaxies, the decline of the EW(H $\delta$ ) is similar for the different galaxy models. The Sd galaxy shows the strongest H $\delta$ -line, because an Sd galaxy at an age of 6 Gyr has a higher gas content than the other spiral models which consume their gas faster and hence allows for the highest burst SFR. Also at an age of 6 Gyr the underlying stellar population before the burst has already a higher EW(H $\delta$ ) than earlier spiral models.

Comparing the three Sa models with the different onset times of 6 Gyr, 9 Gyr and 11 Gyr, Fig. 5 shows that the burst strength reflected in the strength of the H $\delta$ -lines depends strongly on the gas content and its evolution over time. For early bursts, the gas reservoir in the Sa model is still high enough to allow for high burst SFRs and to drive the galaxy to high values of EW(H $\delta$ ) after the burst. At a galaxy age of  $\leq$ 9 Gyr, the gas content of the Sa galaxies is very small because most of the gas has already been converted into stars. Due to the small amount of gas left in the galaxies, only a small starburst can occur at these redshifts and the models do not reach the H $\delta$ -strong regime any more at low redshifts. This helps us to understand why relatively few E+A galaxies are observed at low redshifts.

Fig. 6 compares burst and truncation scenarios and bursts with different decline timescales. In comparison to the burst scenarios, the EW(H $\delta$ ) of the truncation and termination scenarios increases immediately, without dropping first. However, the strength of EW(H $\delta$ ) is much weaker than for galaxies with a preceding burst. In fact only the very strongest cases of the truncation scenario, i.e. the sudden halting of the relatively high SFR in Sc and Sd models, result in EW(H $\delta$ ) values slightly above 5 Å for 0.3 Gyr (Sc) and 0.5

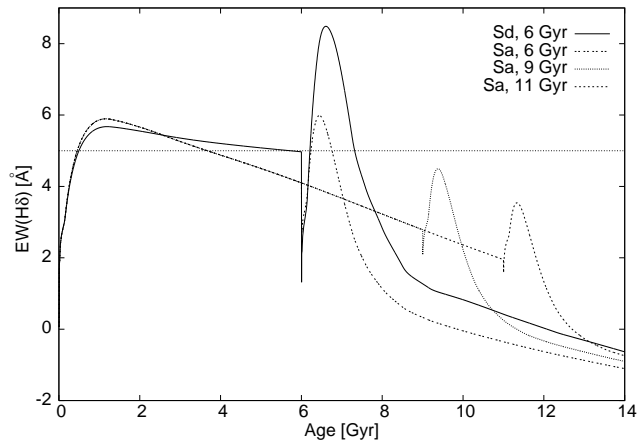


**Figure 5.** Time evolution of EW(H $\delta$ ) in galaxies with different burst scenarios (Sa, burst of 70% at 6 Gyr, decline time 0.1 Gyr; Sd, burst of 70% at 6 Gyr, decline time 0.1 Gyr; Sa, burst of 70% at 11 Gyr, decline time 0.1 Gyr).

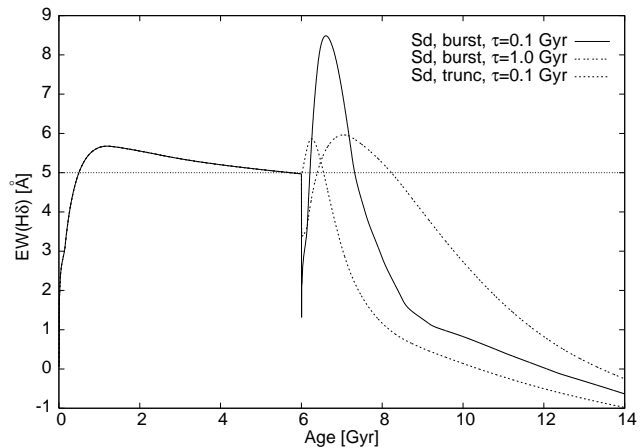


**Figure 6.** Time evolution of EW(H $\delta$ ) in galaxies with different burst scenarios (Sd, burst of 70% at 6 Gyr, decline time 0.1 Gyr; Sd, burst of 70% at 6 Gyr, decline time 1.0 Gyr; Sd, truncation at 6 Gyr, decline time 0.1 Gyr).

Gyr (Sd), while no termination scenario drives the EW(H $\delta$ ) values above the threshold. Compared to the burst scenarios, the H $\delta$ -strong phase of the truncation scenarios starts earlier, e.g. 20 Myr after the onset of SF truncation in an Sd model. Fig. 6 also illustrates on the example of an Sd model that a longer decline time results 1.) in weaker Balmer lines and 2.) possibly in a longer H $\delta$ -strong phase if enough gas is available and therefore the burst SFR can be strong enough for the model galaxy to reach the 5 Å threshold in the post-starburst phase.

The H $\delta$ -strong phase can last up to 2 Gyr in cases with long burst timescales.

The EW(H $\delta$ ) strength does not simply depend on the burst strength, but on a complex interplay of burst strength, decline timescale, onset of the burst and progenitor galaxy type. Depending on the individual model either one of these factors can dominate the influence on the EW(H $\delta$ ).

To study the possible impact of metallicity effects on the H $\delta$ -strength, we run Sd type constant SFR models with different metallicities  $0.0004 \leq Z \leq 0.05$ . The scenarios in Fig. 7 show three

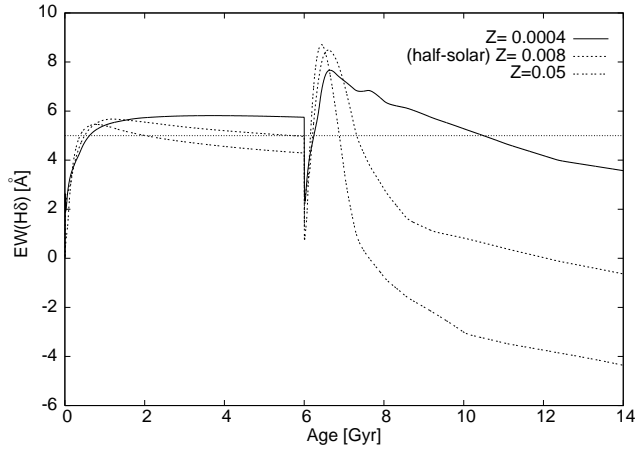


**Figure 7.** Evolution of H $\delta$  with time for Sd models with three different metallicities (Sd, 70% bursts at 6 Gyr, decline times 0.1 Gyr).

bursts at 6 Gyr, a burst strength of  $b=70\%$ , a decline time  $\tau=0.1$  Gyr, but with different metallicities.

It is obvious from Fig. 7 that the EW(H $\delta$ ) depends on the metallicity of the galaxy. While the peak values achieved for EW(H $\delta$ ) are somewhat higher for high metallicity galaxies (EW(H $\delta$ )  $\sim 9$  Å for  $Z=0.05$  versus EW(H $\delta$ )  $\sim 8$  Å for  $Z=0.0004$ ), a low metallicity galaxy remains much longer in the H $\delta$ -strong phase. At low metallicities the stars are generally hotter and brighter. Therefore stars of lower mass populate regions in the HRD that are described by A and early F spectra: For example at solar metallicity the  $1.4 M_{\odot}$  star is the lowest mass reaching into the early F-star range. At low metallicity, longer-living stars down to  $0.9 M_{\odot}$  reach this range and live there for about 4 Gyr. Stars with  $0.9 M_{\odot}$  are much more numerous than  $1.4 M_{\odot}$  stars as a consequence of the stellar IMF. The A-star temperature range in the HRD is reached at solar metallicities by stars  $\geq 1.6 M_{\odot}$  which live there for  $< 1.5$  Gyr. At low metallicities ( $Z < 0.02$ ) these temperatures are already reached by stars  $\geq 1 M_{\odot}$  which live there for  $> 3.8$  Gyr. The life time of an A star increases therefore by a factor  $\geq 2$  at lower metallicities, while additionally there is a higher number of A stars, both acting together to cause a longer H $\delta$ -strong phase. These two effects apparently strongly overcompensate the fact that the lifetime of  $1.5\text{--}3 M_{\odot}$  stars is longer at higher metallicities. The lifetime of stars in this mass range at a metallicity of  $Z=0.05$  is only a factor  $\sim 2$  higher than their lifetime at  $Z=0.0004$  and these high mass stars are much less numerous.

Because galaxies in the early Universe tend to have lower metallicities than galaxies in the local Universe and since a lower metallicity implies a longer H $\delta$ -strong phase, the probability to observe a galaxy in its E+A phase increases towards higher redshifts. Therefore a higher number of E+A galaxies cannot be ascribed solely to a higher number of starburst galaxies but also to the lower metallicities and therefore a longer H $\delta$ -strong phase of galaxies in the early Universe. Higher maximal burst strengths enabled by the higher gas content add to this effect.

In the GALEV code, two different Lick indices for H $\delta$  are implemented, H $\delta_A$  and H $\delta_F$ . The index H $\delta_A$ , which is mainly used in this work has a wider index bandpass and wider pseudo-continuum ranges (Lilly & Fritze 2006). The values of EW(H $\delta_F$ ) are significantly lower at all times than the values of EW(H $\delta_A$ ). Therefore it is very important to check for the consistency of the EW(H $\delta$ ) definitions before comparing with observations of all the Balmer lines

EW(H $\beta$ ), EW(H $\delta$ ) and EW(H $\gamma$ ). The EW(H $\delta$ ) shows the highest values and is therefore easier to measure than the other Balmer lines. Moreover, in contrast to lower order Balmer lines the H $\delta$ -line is less affected by any potential emission line contributions in case of low level residual SF in the galaxy.

### 3.3 H $\delta$ -Strong Galaxies

In this Sect. we will explore those scenarios from our grid which become H $\delta$ -strong and identify the progenitors of the H $\delta$ -strong galaxies.

As shown in Sect. 3.1, all burst scenarios with a burst at 3 Gyr are H $\delta$ -strong since already the undisturbed galaxy models lie above the 5 Å threshold at this time of their evolution (see Fig. 4). For a certain type of progenitor spiral galaxy, the essential parameter to cause an EW(H $\delta$ ) above 5 Å is the peak burst SFR  $\psi_{\text{burst}}$  and not the burst strength. For different spiral progenitors, different peak burst SFRs are required in order to make them H $\delta$ -strong after the burst. For example, all Sa galaxies with a burst SFR  $\psi_{\text{burst}} \geq 15 \frac{M_{\odot}}{\text{yr}}$  become H $\delta$ -strong, while for Sa models with a burst SFR below this value, the EW(H $\delta$ ) does not reach the 5 Å threshold. There are a few exceptions of galaxies which have a value for  $\psi_{\text{burst}}$  above the threshold value for the corresponding galaxy type but do not become H $\delta$ -strong. These exceptions are due to the EW(H $\delta$ ) of the underlying undisturbed galaxy models. Bursts at a later stage in the life of the galaxy cannot cause as strong an H $\delta$ -line, not even for higher SFRs than bursts at earlier times, because the EW(H $\delta$ ) of the underlying undisturbed model is already low. The later the bursts start the lower are the peak values for the EW(H $\delta$ ). The EW(H $\delta$ ) of the underlying galaxy is also responsible for the fact that the different galaxy types have to be examined separately and no global minimal value can be given for a burst SFR to cause an H $\delta$ -strong phase.

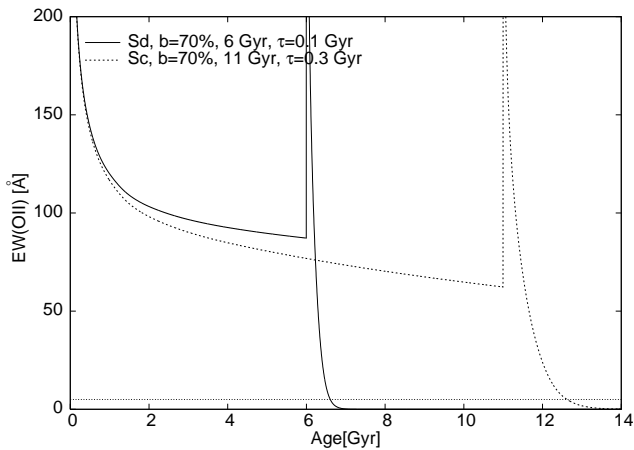
Without exception all Sd models with a burst become H $\delta$ -strong. The maximum value for EW(H $\delta$ ) of 8.5 Å in our sample is reached by the Sd model with a burst of strength  $b=70\%$  at 6 Gyr and a decline time  $\tau=0.1$  Gyr. Almost all Sc burst models become H $\delta$ -strong. Only Sc burst models with long decline time which have moderate to low burst strength and the burst at late galaxy ages do not reach the threshold. Sb burst models with a long decline time do not become H $\delta$ -strong, while all Sb models with a short decline time have a H $\delta$ -strong phase. For Sb burst models with a moderate decline time of 0.3 Gyr it delicately depends on the beginning and the strength of the burst. Most Sa burst models do not become H $\delta$ -strong. Only very few models with early bursts which have short decline times have a H $\delta$ -strong phase.

For the models with SF truncation and termination without a preceding burst only Sc and Sd galaxies can possibly become H $\delta$ -strong. No Sa or Sb truncation or termination model at any galaxy age or with any decline time reaches EW(H $\delta$ )  $\geq 5$  Å. Sc truncation and termination models without a preceding burst only become H $\delta$ -strong, when SF is truncated at early ages and on short timescales, i.e. harassment and strangulation scenarios without a burst can be excluded as possible progenitors for E+A galaxies. In contrast, the Sd models with short and moderate decline times become H $\delta$ -strong. Even an Sd model with a SF termination on a long timescale at early ages has an H $\delta$ -strong phase. Tab. 5 shows a compilation of the H $\delta$ -strong models with starbursts at 9 Gyr.

It can be seen that the later the progenitor galaxy type, the more models become H $\delta$ -strong.

**Table 5.** Compilation of H $\delta$ -strong galaxy models with a burst beginning at 9 Gyr.

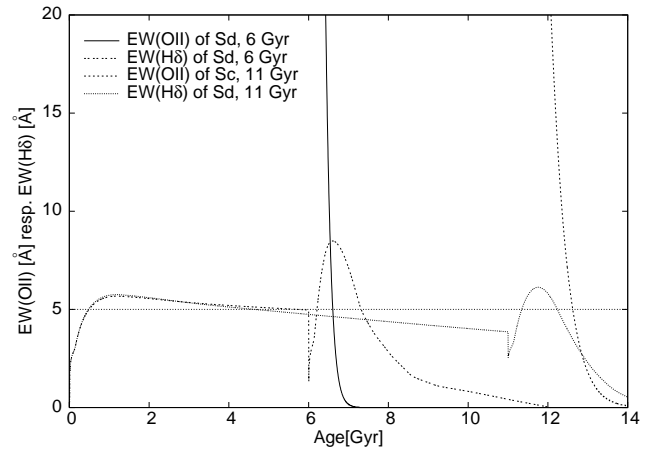
Type	b[%]	$\tau$ [Gyr]
Sa	-	-
Sb	30	0.1
	50	0.1
	70	0.1, 0.3
Sc	30	0.1, 0.3
	50	0.1, 0.3
	70	0.1, 0.3, 1.0
Sd	0	0.1, 0.3
	30	0.1, 0.3, 1.0
	50	0.1, 0.3, 1.0
	70	0.1, 0.3, 1.0

**Figure 8.** Time evolution of EW([O II]) of an Sd galaxy model (Sd, burst 70% at 6 Gyr, decline time 0.1 Gyr) and an Sc galaxy model (Sc, burst 70% at 11 Gyr, decline time 0.3 Gyr).

### 3.4 [O II]-Lines of H $\delta$ -Strong Galaxies

The second important criterion for a galaxy to be classified as E+A galaxy is to ensure that the galaxy has no current SF by measuring the EW([O II]) at 3727 Å. For this purpose we modelled the EW([O II]) on the basis of the SFR and B-band luminosity using a relation given by Kennicutt (1992b) as introduced in Sect. 2.3. In Fig. 8, the time evolution of the EW([O II]) of an Sd galaxy with a burst of 70%, an onset at 6 Gyr and a decline time of 0.1 Gyr, and of an Sc galaxy with a burst of 70%, an onset at 11 Gyr and a decline time of 0.3 Gyr is shown. The EW([O II]) increases instantly at the onset of the burst and afterwards decreases rapidly.

It is obvious that the EW([O II]) reflects the time evolution of the SFR. It is to note, however, that the EW([O II]) remains at high values for some time after the burst and therefore extends into parts of the H $\delta$ -strong phase, as can be seen in Fig. 9 for the Sd and Sc galaxy models described above. In this Fig., the time evolution of EW([O II]) is plotted together with the time evolution of EW(H $\delta$ ). The peaks of the EW([O II]) are not shown in this figure, because the values are much higher than EW(H $\delta$ ) during the burst and would make it impossible to see the EW(H $\delta$ ) in the same plot. The horizontal line marks the thresholds for EW(H $\delta$ ) as well as for EW([O II]). The threshold for EW([O II]) is chosen to be 5 Å, i.e.

**Figure 9.** Time evolution of EW([O II]) and EW(H $\delta$ ) of an Sd galaxy model (Sd, burst 70% at 6 Gyr, decline time 0.1 Gyr) and an Sc galaxy model (Sc, burst 70% at 6 Gyr with decline time 0.3 Gyr).

at the upper limit for this threshold from Dressler et al. (1999). We chose this upper limit taking into account that observed spectra always have noise, which tends to bias observed EW([O II]) towards lower values, while we calculated the EW([O II]) from the SFR.

The Sd galaxy in Fig. 9 is the model with the longest E+A phase of 0.71 Gyr in our grid. It is the same galaxy that has the strongest peak value for EW(H $\delta$ ) in our sample. The beginning of the E+A phase is given by the drop of EW([O II]) below 5 Å, while the end of the E+A phase is defined by the drop of EW(H $\delta$ ) below 5 Å. The duration of the E+A phase thus amounts only 64% of the H $\delta$ -strong phase with a duration of 1.11 Gyr. This example shows that the E+A phase only accounts a dramatically short fraction of the post-starburst phase. For many galaxy models, the phase of strong [O II] emission is even longer than the H $\delta$ -strong phase as demonstrated in the left of Fig. 9. The H $\delta$ -strong phase of the Sc galaxy model is already over when the EW([O II]) drops below 5 Å and this model therefore would not be classified as an E+A galaxy.

It is striking that the models can clearly be separated according to the different decline times from looking at the strength of EW([O II]). *All H $\delta$ -strong galaxy models with SFR decline times of 0.1 Gyr have an E+A phase, i.e. sufficient low [O II]-lines during their H $\delta$ -strong phase, while all models with SFR decline times of 1.0 Gyr and 0.3 Gyr never go through an E+A phase since they still have [O II] emission during their H $\delta$ -strong phase.*

Therefore we state that the conventional definition of E+A galaxies based on the absence of [O II] emission above some threshold is too narrow to encompass the full range of post-starburst galaxies. In particular, galaxies with a long decline time are excluded since they exhibit significant [O II] emission in addition to their strong Balmer absorption lines. Possible processes leading to E+A galaxies can only be galaxy mergers and gas stripping (with a starburst), while harassment and strangulation can be excluded due to their long decline timescales.

### 3.5 Spectral evolution of E+A Galaxies

Figs. 10 to 13 show spectra of the galaxy models with the highest and the lowest peak value for EW(H $\delta$ ). The highest value is reached by the Sd model with a burst strength  $b=70\%$ , an onset at 6 Gyr and a decline time of  $\tau=0.1$  Gyr (see Sect. 3.2), shown on the top of Figs. 10 to 13. The bottom of Figs. 10 to 13 shows the Sa



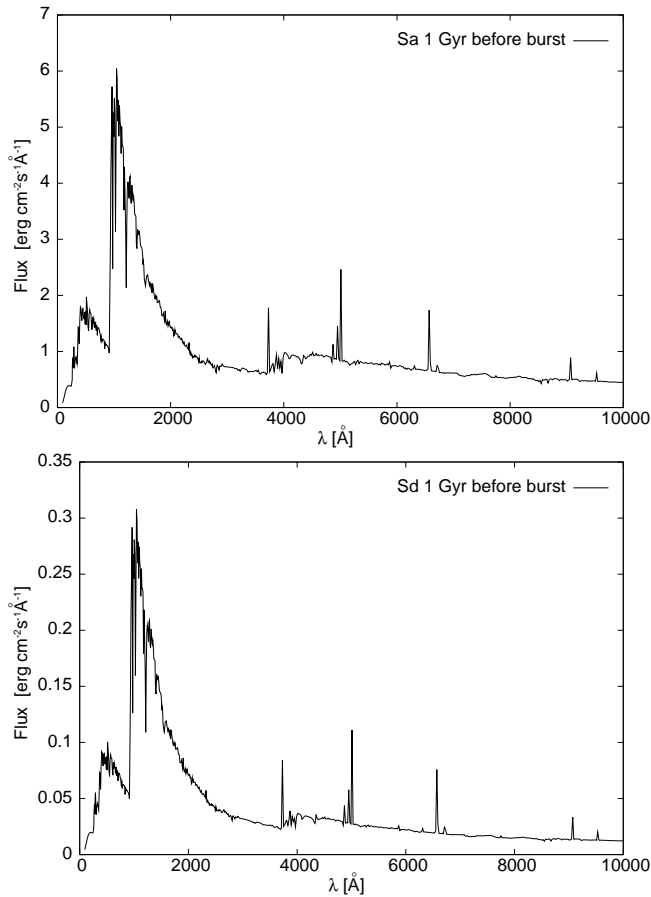


**Figure 10.** Spectra of an Sa model (burst 50%) and an Sd model (burst 70%) 1 Gyr before the bursts (at 6 Gyr, decline times 0.1 Gyr).

model with a burst strength  $b=50\%$ , an onset at 6 Gyr and a decline time  $\tau=0.1$  Gyr, which has the lowest value for  $EW(H\delta)$  of all our galaxy models classified as E+A. Note the different flux scales in all graphs of Figs. 10 to 13. The different stages of the galaxies in these figures are given in relation to the onset of the burst. The two graphs in Fig. 10 show the spectra of the Sd and Sa burst models at an age of 5 Gyr, i.e. 1 Gyr before the burst starts. Therefore the galaxies have spectra of normal undisturbed Hubble type Sd and Sa galaxies at that age. The graphs in Fig. 11 show the same galaxies during their bursts at an age of 6 Gyr. The spectra show much stronger emission lines and a higher UV flux than the undisturbed galaxies.

In Fig. 12 the  $H\delta$ -strong phase of the two models is shown. The spectra show the galaxies at the age, when the  $EW(H\delta)$  has reached its maximum value (i.e. at 6.6 Gyr for the Sd, and at 6.4 Gyr for the Sa model) and at an age of 7 Gyr, i.e. 1 Gyr after the burst. In Tab. 6 the corresponding line strengths for  $EW(H\delta)$  and  $EW([O\text{II}])$  are listed for these spectra. We recall that our spectra do not have enough resolution to measure the line strength. The values for the line strengths of  $EW(H\delta)$  and  $EW([O\text{II}])$  listed here are calculated as described in Sect. 2.3 and 2.2.

The spectra at 6.6 Gyr and 6.4 Gyr, respectively, still have high UV fluxes and the overall continuum does not yet look like a typical passive galaxy spectrum but instead resembles an A-star spectrum. In comparison, the two spectra look rather different, especially when looking at the regions around the Lyman- $\alpha$ -line at 1216 Å and the 4000 Å break. The Balmer lines are stronger in the

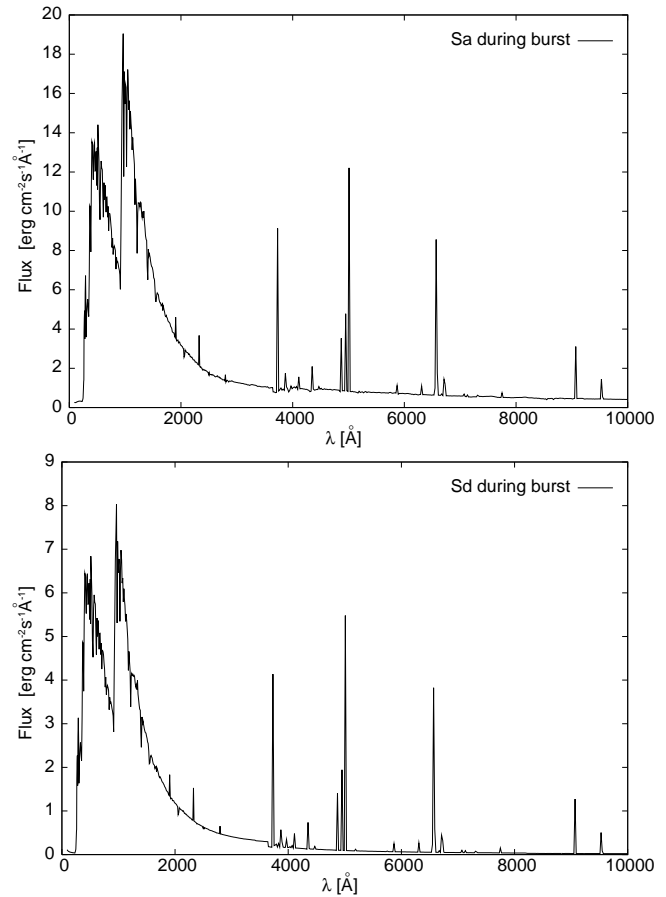


**Figure 11.** Spectra of an Sa model (burst 50%) and an Sd model (burst 70%) during the burst (at 6 Gyr, decline times 0.1 Gyr).

**Table 6.** Values of  $EW(H\delta)$  and  $EW([O\text{II}])$  for an Sd model (top) with a burst strength of 70% and an Sa model (bottom) with burst strength of 50%, both with an onset at 6 Gyr and a decline timescale of 0.1 Gyr.

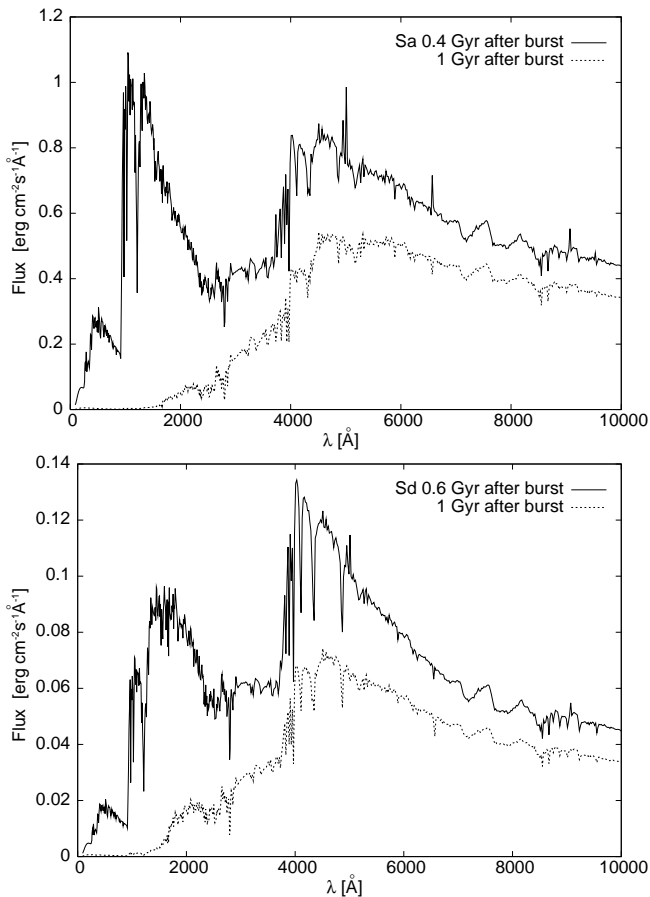
Sd	Age	$EW(H\delta)[\text{Å}]$	$EW([O\text{II}])[Å]$
	6.6	8.5	4.9
	7.0	7.1	0.2
	9.0	1.3	-

Sa	Age	$EW(H\delta)[Å]$	$EW([O\text{II}])[Å]$
	6.4	5.6	11.7
	7.0	3.4	0.1
	9.0	0.3	-

Sd galaxy and no significant emission lines can be seen. In fact, the Sd galaxy at 6.6 Gyr has an  $EW([O\text{II}])$  lower than 5 Å and would be classified as an E+A galaxy. However, its spectrum at the bottom of Fig. 12 does not look like a typical E+A spectrum, i.e. like a spectrum of a passive galaxy with significant A-star features, particularly when looking at the UV flux. This confusion is due to the fact that in the literature, spectra of E+A galaxies do not reach into the UV region, which, however, is the wavelength range with the strongest changes during the post-starburst phase.

The Sa model has strong  $[O\text{II}]$  emission lines for a longer time after the burst, while its values for  $EW(H\delta)$  are weaker and drop



**Figure 12.** Spectra of an Sa model (burst 50%) and an Sd model (burst 70%) in the burst (at 6 Gyr, decline times 0.1 Gyr). The spectra show the galaxies in their post-starburst phase at their maximum EW( $H\delta$ ) and 1 Gyr after the burst.

faster than in the Sd model. In contrast to the Sd model, the Sa galaxy at 6.4 Gyr still has an  $\text{EW}([\text{O II}]) \geq 5 \text{ \AA}$ , as shown in Tab. 6. Its spectrum 1 Gyr after the burst looks like a typical passive spectrum with a superposition of A-star features. The UV flux is very low and the Lyman- $\alpha$ -line at  $1216 \text{ \AA}$  has disappeared. No emission lines can be seen, while the Balmer lines and the  $4000 \text{ \AA}$  break are present, even though  $\text{EW}(H\delta) \leq 5 \text{ \AA}$  for the Sa galaxy model (see Tab. 6). From the continuum ratios as well as from the strengths of the Balmer lines and the  $4000 \text{ \AA}$  break the different burst scenarios are distinguishable.

The spectra in Fig. 13 show the galaxy models after the E+A phase, at a galaxy age of 9 Gyr. Now, 3 Gyr after the burst both spectra look like true passive galaxy spectra and the Balmer lines have disappeared. We conclude that studying E+A galaxies over a larger wavelength range, particularly including the UV range, promises a better discrimination of progenitor galaxies and transformation scenarios than only looking at  $\text{EW}(H\delta)$  and  $\text{EW}([\text{O II}])$ . Our results also indicate that the analysis of Spectral Energy Distributions (SEDs) extending from UV/U trough optical and eventually NIR passbands will allow to encompass all post-starburst phases, even those, which are excluded from the classical E+A definition based on the optical region only. This will be investigated Paper II.

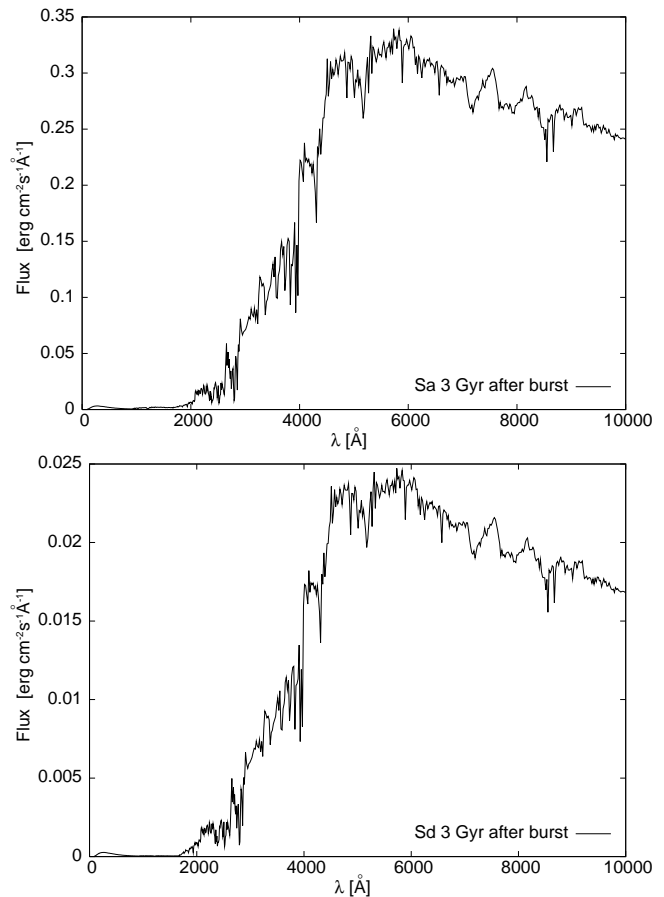


**Figure 13.** Spectra of an Sa model (burst 50%) and an Sd model (burst 70%) after their post-starburst phase, 3 Gyr after the bursts (at 6 Gyr, decline times 0.1 Gyr).

### 3.6 Comparison with Template Spectra

In Figs. 14 to 16, different ages of the Sa galaxy model with a burst onset at 6 Gyr, a burst strength of 50% and a decline time of 0.1 Gyr are shown together with the E+A galaxy template from Kennicutt (1992a). Fig. 14 shows the Sa model 0.4 Gyr after the burst. At this age, the model spectrum is still too young to match the template. The flux between  $4000$  and  $5000 \text{ \AA}$  is still too high. When we look at Fig. 15, we can see that 0.7 Gyr after the burst the flux decreased enough to match the template very well. A little later, 1 Gyr after the burst, the flux between  $4000$  and  $5000 \text{ \AA}$  is already too low as compared to the template continuum. Fig. 17 shows the same Sa galaxy model 7 Gyr after the burst, compared to Kennicutt's E galaxy template. The model has passed the E+A phase and matches the template of an E galaxy very well.

In Figs. 18 and 19, we compare the Sd model with a burst of 70%, an onset at 6 Gyr and a decline time of 0.1 Gyr with Kennicutt's E+A and E templates, respectively. Shown are the Sd model spectra at the times when they best match.

It is obvious that, in general, the model spectra match the templates very well, however not quite as well as the Sa model spectra. This result is inline with investigations of NGC 3921 in the literature. It is proposed that NGC 3921 is a merger remnant of two disk galaxies, Sa and Sc, with a burst  $0.7 \pm 0.3$  Gyr ago, which is expected to evolve into a normal elliptical galaxy on a timescale of

Our comparison of E+A galaxy spectra several Gyr after the starburst with template spectra of E and S0 galaxies shows that

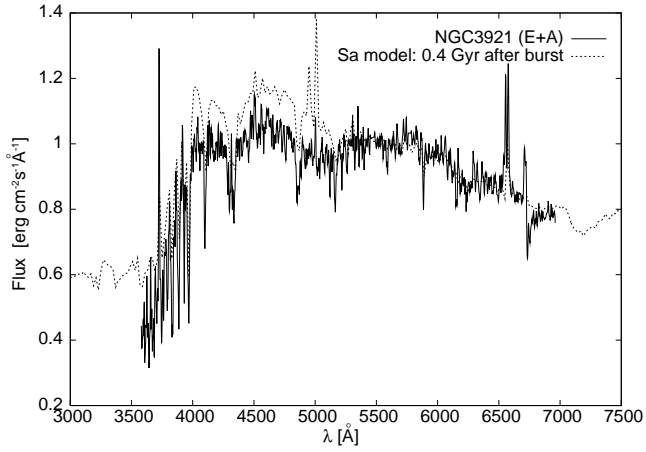


**Figure 14.** Spectra of an Sa model shown 0.4 Gyr after a burst and an E+A template from Kennicutt (1992a) (Sa, burst 50% at 6 Gyr, decline time 0.1 Gyr).

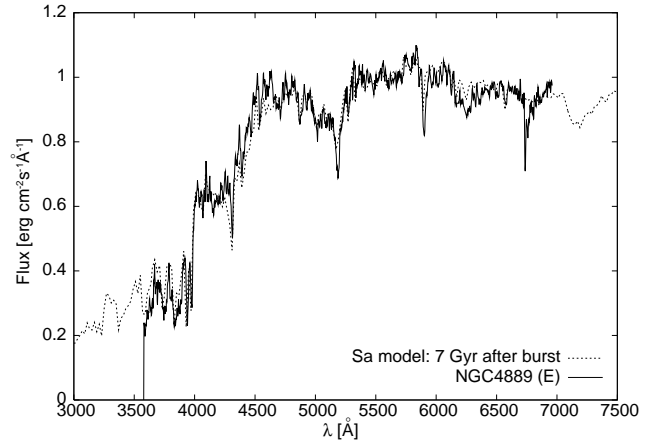


**Figure 17.** Spectra of an Sa model shown 7 Gyr after a burst and an E template from Kennicutt (1992a) (burst 50% at 6 Gyr, decline time 0.1 Gyr).

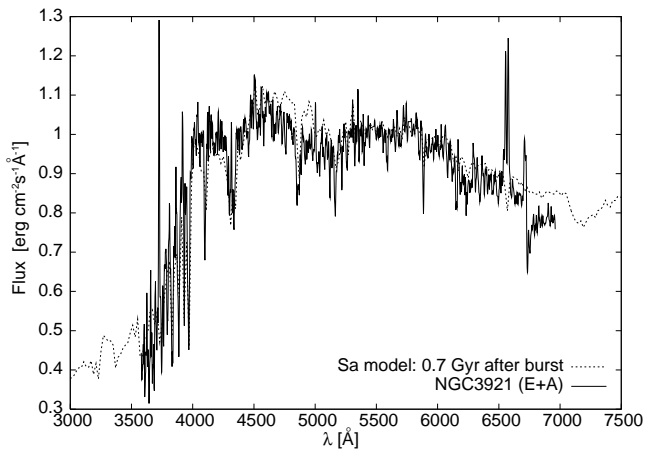


**Figure 15.** Spectra of an Sa model shown 0.7 Gyr after a burst and an E+A template from Kennicutt (1992a) (burst 50% at 6 Gyr, decline time 0.1 Gyr).

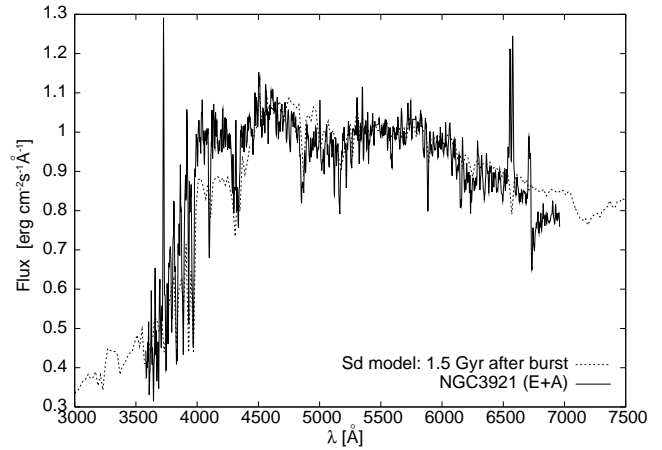


**Figure 18.** Spectra of an Sd model shown 1.5 Gyr after a burst and an E+A template from Kennicutt (1992a) (burst 70% at 6 Gyr, decline time 0.1 Gyr).

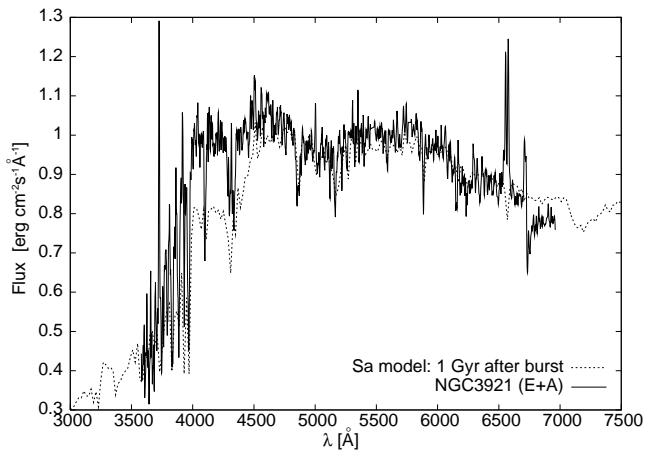


**Figure 16.** Spectra of an Sa model shown 1 Gyr after a burst and an E+A template from Kennicutt (1992a) (burst 50% at 6 Gyr, decline time 0.1 Gyr).

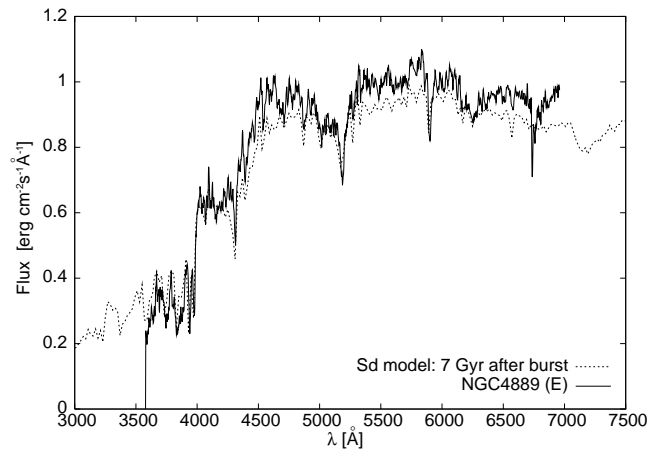


**Figure 19.** Spectra of an Sd model shown 7 Gyr after a burst and an E template from Kennicutt (1992a) (burst 70% at 6 Gyr, decline time 0.1 Gyr).

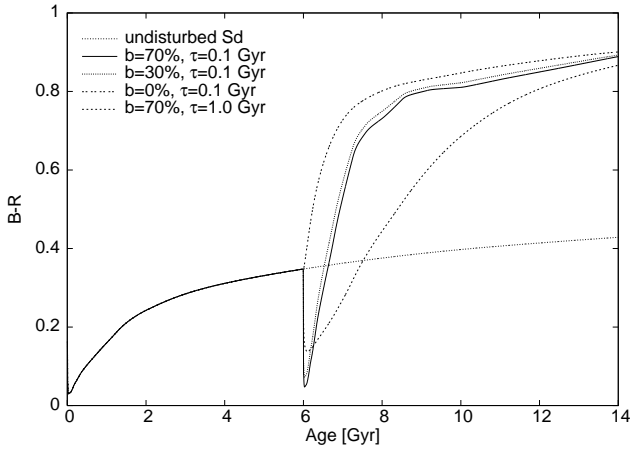


**Figure 20.** Time evolution of B–R for Sd models with different burst strengths (Sd, burst beginning at 6 Gyr, decline time 0.1 Gyr).

E+A evolve into early-type galaxies in agreement with investigations from Bicker et al. (2003) of the origin of S0 galaxies in clusters.

### 3.7 B–R Color of Post-Starburst Galaxies

In Fig. 20 three Sd models with the same onset of the burst at 6 Gyr, the same decline timescale of  $\tau=0.1$  Gyr but different burst strength (70%, 30% and 0%, i.e. SF truncation) are presented as well as an Sd model with an onset at 6 Gyr and a decline timescale of  $\tau=1.0$  Gyr with a burst strength of 70%. For comparison an undisturbed Sd model is shown. We recall that the scenario with the long decline timescale does not lead to an E+A phase because it shows significant [O II]-lines during its H $\delta$ -strong phase. A burst causes the galaxies to become very blue before they get red due to the truncation/termination of SF. The models with SF truncation or termination only quickly become red immediately after the onset. Therefore up to 12 Gyr the models with a starburst before the halting of SF are bluer. Late type spiral galaxies are in general bluer than early type galaxies and therefore take longer to become red. For old ages all burst and SF truncation/termination scenarios converge to similar colors as the age differences between their stellar populations become more and more negligible and the photometry of the galaxies is dominated by stars of the Red Giant Branch and Asymptotic Giant Branch.

The decline timescale of the burst has a strong effect on how fast the galaxy model becomes red after the burst. The model with a long decline time of 1.0 Gyr is bluer than the undisturbed model for almost 2 Gyr, while the model with the shortest decline timescale of 0.1 Gyr is already redder than the undisturbed model after about 0.5 Gyr. The symbols mark 1 Gyr intervals. In Fig. 21 the EW(H $\delta$ ) is plotted against the color B–R. With this plot it is possible to investigate the evolution in color during the H $\delta$ -strong phase. It is possible to see which galaxy models become red during their H $\delta$ -strong phase and which remain blue. Since blue as well as red E+A galaxies have been observed this investigation is of great interest (Yang et al. 2008; Zabudoff et al. 1996). The horizontal line is the 5 Å threshold, separating H $\delta$ -strong from non H $\delta$ -strong models, while the vertical line at B–R=1.1 separates blue (to the left) from red galaxies (on the right).

The value of 1.1 for the limit was chosen to lie between the values of the undisturbed Sb and Sc models at a galaxy age of 13

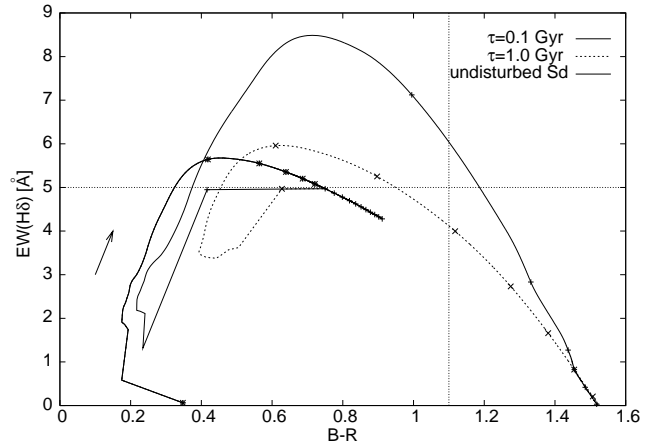


**Figure 21.** EW(H $\delta$ ) versus B–R of two Sd models with different decline times (Sd, burst 70% at 6 Gyr).

Gyr, i.e. at redshift  $z=0$ . Model in the upper right square are red during their H $\delta$ -strong phase. The arrow points into the direction in which the models evolve with time.

In Fig. 21 two Sd models with the same burst strength of 70% and an onset at 6 Gyr but different decline times  $\tau$  (0.1 and 1.0 Gyr) are shown together with the undisturbed Sd model. Again it has to be remarked that the model with the long decline time is not an E+A galaxy. The burst models separate from the undisturbed model after the 6 Gyr mark due to the rapid change in color at the onset of the burst. At the beginning of the burst, the color starts to change faster than the EW(H $\delta$ ). The model with the decline time of 1.0 Gyr falls already under the 5 Å threshold before it reaches the red side, i.e. it spends all of its H $\delta$ -strong phase in the blue. The model with a shorter decline time of 0.1 Gyr crosses the blue-red border while still H $\delta$ -strong. It is observable both in a blue and in a red H $\delta$ -strong phase because the value for EW(H $\delta$ ) of the model with decline time 0.1 Gyr reaches a high peak value for EW(H $\delta$ ) and drops slower below 5 Å than the color evolves towards the red. The two models in Fig. 21 are representative for all models of our grid. Hence *all E+A galaxy models with short decline times become red, while models with long decline times (not E+A!) always stay blue and do not cross the color threshold.*

For models with a decline time of 0.3 Gyr it depends on the time when the burst occurs whether they get red during their H $\delta$ -strong phase or not. All models with a decline time of 0.3 Gyr and an onset at 11 Gyr become red during their H $\delta$ -strong phase, while models with a decline time of 0.3 Gyr and an onset at 9 and 6 Gyr can show either behavior. Some of these models have stronger values for EW(H $\delta$ ) and become red during their H $\delta$ -strong phase, while others have EW(H $\delta$ ) only marginally above the 5 Å threshold and do not stay H $\delta$ -strong long enough to have a red H $\delta$ -strong phase.

We conclude, that the later the type and the longer the decline time, the longer it takes for the models to become red. Red post-starburst galaxies are possibly a later stage of blue post-starburst galaxies with a strong burst, i.e. a merger or gas stripping scenario in a late stage. Scenarios that terminate the SFR on a long timescale, like those associated with harassment and strangulation, or scenarios with an intermediate decline time with a weak burst can be excluded for red H $\delta$ -strong galaxies.

By looking at the colors of H $\delta$ -strong galaxies we can constrain their decline times. This result let us assume that these sce-



narios are distinguishable by comparing the SEDs of post-starburst galaxies as investigated in Paper II.

#### 4 CONCLUSIONS AND OUTLOOK

We investigated the transformation of galaxies when entering a high density environment like a galaxy cluster. In particular we focused on the E+A galaxy class, which contains galaxies in an important transition stage, a post-starburst phase, of galaxy transformation. E+A galaxies are defined to have strong Balmer absorption lines but no significant emission lines. The spectrum of an E+A galaxy therefore looks like a superposition of the passive spectrum of an elliptical galaxy and deep Balmer absorption lines typical for A-stars. We examined the different processes of galaxy transformation like mergers, harassment, gas stripping and strangulation in terms of their impact on the SF history of galaxies and identified the most likely progenitors and successors of E+A galaxies. For this purpose, we used the GALEV galaxy evolution code to calculate a grid of spiral galaxy models with different combinations of a starburst, i.e. a sudden increase of the star formation rate (SFR), and a halting of the SFR on different timescales, i.e. SF truncation and termination. With these scenarios it is possible to describe the effects on the SFR of the four different galaxy transformation scenarios mentioned above. We varied the amount of gas consumed in the starburst (burst strength) and the galaxy age at which the starburst, the SF truncation or termination begins (onset). The spectra and colors as well as the time evolution of Lick indices, in particular the EW(H $\delta$ ) of the H $\delta$  absorption line at 4100 Å and the EW([O II]) of the [O II] emission line at 3727 Å as indicators of recent and ongoing SF were modelled and discussed.

When investigating the time evolution of the EW(H $\delta$ ), we found that the EW(H $\delta$ ) is the result of a complex interplay of burst strength, decline timescale, onset of the burst and progenitor galaxy type:

(i) The later the *progenitor galaxy type*, the easier an H $\delta$ -strong phase is reached. All Sd burst models become H $\delta$ -strong and the maximum value for EW(H $\delta$ ) is reached by an Sd model. For a certain type of progenitor spiral galaxy, the essential parameter to cause an EW(H $\delta$ ) above 5 Å is the peak burst SFR  $\psi_{\text{burst}}$  with different values for each spiral type.

(ii) The earlier the *onset* of the burst, the higher are the peak values reached by the EW(H $\delta$ ). For bursts beginning at a galaxy age of 3 Gyr all scenarios are H $\delta$ -strong due to the larger available gas reservoir at such young ages.

(iii) The longer the *decline timescale* of the SFR after a burst, the lower are the values reached for EW(H $\delta$ ), but the longer is the duration of the H $\delta$ -strong phase. The H $\delta$ -strong phase can last up to 2 Gyr in cases of long decline timescales.

(iv) The higher the *burst strength*, the higher are the peak values for the EW(H $\delta$ ). Only very few scenarios with a truncation or termination of SF without a preceding burst have a H $\delta$ -strong phase. Those are the late-type spirals with their relatively high SFRs and a truncation on a short timescale. They have EW(H $\delta$ ) slightly above 5 Å for a short time.

We find a significant effect of the metallicities in galaxies on their EW(H $\delta$ ) and conclude that a higher number of E+A galaxies at high redshift cannot be ascribed solely to a higher number of starburst galaxies but also to the lower metallicities of galaxies that cause longer H $\delta$ -strong phases in the early universe and to the higher burst strengths enabled by the higher gas content.

A striking result are the values for EW(H $\delta$ ) that we found for undisturbed galaxies. We discovered that galaxies, which only follow the normal evolution, all go through a phase between ages of 1.5 and 6 Gyr in which they have strong H $\delta$ -lines. Not taking this result into account in analyses of high redshift galaxies leads to an underestimation of emission lines, which are influenced by the Balmer absorption lines, for example the H $\alpha$ -line and H $\beta$ , and of the SFR derived from those.

By investigating the second criterion for E+A galaxies, the [O II] emission line at 3727 Å, we found that the selection criteria for E+A galaxies commonly used exclude a significant number of post-starburst galaxies, in particular those galaxies with a long decline time. The conventional definition of an E+A galaxy is too narrow to encompass the full range of post-starburst galaxies. Possible progenitors of E+A galaxies can only be galaxy mergers and maybe galaxies with gas stripping with a starburst, while the processes of harassment and strangulation can be excluded due to the long decline timescales they induce for SF.

The comparison of E+A galaxy spectra several Gyr after the starburst with template spectra of E and S0 galaxies showed that the successors of E+A galaxies are early-type galaxies. From our model spectra of E+A galaxies, we predict that studying E+A galaxies over a larger wavelength range, particularly including the UV, yields a better discrimination of progenitor galaxies and transformation scenarios. The analysis of Spectral Energy Distributions (SEDs) will allow to encompass all post-starburst phases, even those which are excluded from the classical E+A definition based on optical regions only. From our investigation of the time evolution of the B–R colors of our post-starburst galaxy models we found, that the progenitor galaxy type and the decline time have the greatest effects on the color evolution. The later the type and the longer the decline time, the longer it takes for the models to become red. Red E+A galaxies and red post-starburst galaxies in general are possibly a later stage of blue post-starburst galaxies with a strong burst and a short or intermediate decline time as e.g. triggered by a merger. Galaxy models with an intermediate decline time ( $\geq 0.3$  Gyr) with a weak burst and models with a long decline time ( $\geq 1.0$  Gyr) no matter how strong a burst was do not become red during their H $\delta$ -strong phase. Our results from examining the spectra and the colors of post-starburst galaxies indicate that it is possible to select and distinguish post-starburst galaxies by looking at their Spectral Energy Distributions (SEDs), which will be presented in Paper II.

We have shown that E+A galaxies by definition include only transformation processes on a short timescale. The full range of post-starburst galaxies have not yet been investigated observationally. This needs to be done in order to achieve a comprehensive understanding of the galaxy transformation processes in high density environments.

#### ACKNOWLEDGMENTS

We would like to thank the referee for very useful comments and suggestions.

#### REFERENCES

- Anders P., Fritze-v. Alvensleben U., 2003, A&A, 401, 1063
- Balogh M. L., Miller C., Nichol R., Zabludoff A., Goto T., 2005, MNRAS, 360, 587

- Balogh M. L., Morris S. L., Yee H. K. C., Carlberg R. G., Ellingson E., 1999, *ApJ*, 527, 54
- Barger A. J., Aragon-Salamanca A., Ellis R. S., Couch W. J., Smail I., Sharples R. M., 1996, *MNRAS*, 279, 1
- Bekki K., Couch W. J., Shioya Y., Vazdekis A., 2005, *MNRAS*, 359, 949
- Bertelli G., Bressan A., Chiosi C., Fagotto F., Nasi E., 1994, *A&AS*, 106, 275
- Bicker J., Fritze-v. Alvensleben U., Möller C. S., Fricke K. J., 2004, *A&A*, 413, 37
- Bicker J., Fritze-von Alvensleben U., Fricke K. J., 2003, *Ap&SS*, 284, 463
- Bravo-Alfaro H., Cayatte V., van Gorkom J. H., Balkowski C., 2000, *AJ*, 119, 580
- Butcher H., Oemler Jr. A., 1978, *ApJ*, 226, 559
- Butcher H., Oemler Jr. A., 1984, *ApJ*, 285, 426
- Buyle P., De Rijcke S., Dejonghe H., 2008, *ArXiv:0807.0440*
- Cayatte V., van Gorkom J. H., Balkowski C., Kotanyi C., 1990, *AJ*, 100, 604
- Chang T.-C., van Gorkom J. H., Zabludoff A. I., Zaritsky D., Mihos J. C., 2001, *AJ*, 121, 1965
- Couch W. J., Ellis R. S., Sharples R. M., Smail I., 1994, *ApJ*, 430, 121
- Couch W. J., Sharples R. M., 1987, *MNRAS*, 229, 423
- Dressler A., 1980, *ApJ*, 236, 351
- Dressler A., Oemler A. J., Butcher H. R., Gunn J. E., 1994, *ApJ*, 430, 107
- Dressler A., Oemler A. J., Couch W. J., Smail I., Ellis R. S., Barger A., Butcher H., Poggianti B. M., Sharples R. M., 1997, *ApJ*, 490, 577
- Dressler A., Smail I., Poggianti B. M., Butcher H., Couch W. J., Ellis R. S., Oemler A. J., 1999, *ApJS*, 122, 51
- Ellingson E., Lin H., Yee H. K. C., Carlberg R. G., 2001, *ApJ*, 547, 609
- Falkenberg M. A., Kotulla R., Fritze U., 2009, submitted to *MNRAS*
- Fasano G., Poggianti B. M., Couch W. J., Bettoni D., Kjærgaard P., Moles M., 2000, *ApJ*, 542, 673
- Gavazzi G., Cortese L., Boselli A., Iglesias-Paramo J., Vílchez J. M., Carrasco L., 2003, *ApJ*, 597, 210
- Girardi L., Bertelli G., Bressan A., Chiosi C., Groenewegen M. A. T., Marigo P., Salasnich B., Weiss A., 2003, *Memorie della Societa Astronomica Italiana*, 74, 474
- Gómez P. L., Nichol R. C., Miller C. J., Balogh M. L., Goto T., Zabludoff A. I., Romer A. K., Bernardi M., Sheth R., Hopkins A. M., Castander F. J., Connolly A. J., Schneider D. P., Brinkmann J., Lamb D. Q., SubbaRao M., York D. G., 2003, *ApJ*, 584, 210
- Goto T., 2004, *A&A*, 427, 125
- Gunn J. E., Gott J. R. I., 1972, *ApJ*, 176, 1
- Helmboldt J. F., 2007, *MNRAS*, 379, 1227
- Kaviraj S., Kirkby L. A., Silk J., Sarzi M., 2007, *MNRAS*, 382, 960
- Kennicutt Jr. R. C., 1992a, *ApJS*, 79, 255
- Kennicutt Jr. R. C., 1992b, *ApJ*, 388, 310
- Kodama T., Bower R. G., 2001, *MNRAS*, 321, 18
- Lejeune T., Cuisinier F., Buser R., 1998, *A&AS*, 130, 65
- Leonardi A. J., Rose J. A., 1996, *AJ*, 111, 182
- Lilly T., Fritze U. F.-V., 2006, *A&A*, 457, 467
- Liu C. T., Hooper E. J., O'Neil K., Thompson D., Wolf M., Lisker T., 2007, *ApJ*, 658, 249
- Mihos J. C., 2004, in *Mulchaey J. S., Dressler A., Oemler A., eds, Clusters of Galaxies: Probes of Cosmological Structure and Galaxy Evolution Interactions and Mergers of Cluster Galaxies.* pp 277–+
- Moore B., Lake G., Katz N., 1998, *ApJ*, 495, 139
- Oemler A. J., 1974, *ApJ*, 194, 1
- Poggianti B., 2004, in *Dettmar R., Klein U., Salucci P., eds, Baryons in Dark Matter Halos Evolution of galaxies in clusters*
- Poggianti B. M., Barbaro G., 1996, *A&A*, 314, 379
- Poggianti B. M., Bridges T. J., Komiyama Y., Yagi M., Carter D., Mobasher B., Okamura S., Kashikawa N., 2004, *ApJ*, 601, 197
- Quilis V., Moore B., Bower R., 2000, *Science*, 288, 1617
- Richstone D. O., 1976, *ApJ*, 204, 642
- Sandage A., Binggeli B., Tammann G. A., 1985, *AJ*, 90, 1759
- Toomre A., Toomre J., 1972, *ApJ*, 178, 623
- Trager S. C., Worthey G., Faber S. M., Burstein D., Gonzalez J. J., 1998, *ApJS*, 116, 1
- Tremonti C. A., Heckman T. M., Kauffmann G., Brinchmann J., Charlot S., White S. D. M., Seibert M., Peng E. W., Schlegel D. J., Uomoto A., Fukugita M., Brinkmann J., 2004, *ApJ*, 613, 898
- Verdugo M., Ziegler B. L., Gerken B., 2008, *A&A*, 486, 9
- Worthey G., Faber S. M., Gonzalez J. J., Burstein D., 1994, *ApJS*, 94, 687
- Worthey G., Ottaviani D. L., 1997, *ApJS*, 111, 377
- Yang Y., Zabludoff A. I., Zaritsky D., Lauer T. R., Mihos J. C., 2004, *ApJ*, 607, 258
- Yang Y., Zabludoff A. I., Zaritsky D., Mihos J. C., 2008, *ApJ*, 688, 945
- Zabludoff A. I., Zaritsky D., Lin H., Tucker D., Hashimoto Y., Shectman S. A., Oemler A., Kirshner R. P., 1996, *ApJ*, 466, 104
- Zaritsky D., Kennicutt Jr. R. C., Huchra J. P., 1994, *ApJ*, 420, 87